On a one-dimensional shape-memory alloy model in its fast-temperature-activation limit

Toyohiko Aiki*, Martijn Anthonissen†, Adrian Muntean‡

June 18, 2009

Abstract

We study a one-dimensional model describing the motion of a shape-memory alloy spring at a small characteristic time scale, called here *fast-temperature-activation limit*. At this level, the standard Falk's model reduces to a nonlinear elliptic partial differential equation (PDE) with Newton boundary condition. We show existence and uniqueness of a bounded weak solution and approximate this numerically. Interestingly, in spite of the nonlinearity of the model, the approximate solution exhibits nearly a linear profile. Finally, we extend the reduced model to the simplest PDE system for shape memory alloys that can capture oscillations and then damp out these oscillations numerically. The numerical results for both limiting cases show excellent agreement. The graphs show that the valve opens in an instant, which is realistic behavior of the free boundary.

1 Introduction

A shape memory alloy (SMA, also known as a smart metal) is a material that "remembers" its shape. More precisely, by applying heat to alloys like Fe-Mn-Si or Ni-Ti, they can be returned to the initial shape after being deformed. As a result of sensitive responses to typically small temperature vibrations, such materials are currently employed for instance in micro- and nano-machinery, aerospace technology, self-repairing shielding devices, and biomedical implants. It is worth mentioning that, also due to their usually low production costs, SMA are particularly attractive from the applications point of view[1]. Note however that although the alloy components are well understood, many of the SMA effects are still not yet completely understood from theoretical perspectives. We refer the reader to [2, 4], e.g., and references therein for a partial list of open mathematical problems.

Our primary concern is to find simulation strategies to damp the unwanted oscillations inherently occurring in the simulation of coupled SMA-elastic spring devices. In this spirit, the departure point of this paper is the following problem modeling the motion of a shape-memory alloy spring having density $\rho_1 > 0$ coupled with a linear elastic spring of density $\rho_2 = 0$. This problem, see (1)–(9) below, is a particular case of a more general scenario, sometimes called Falk's model, presented in [1]. For details on modeling and mathematical aspects related to the Falk's model for shape-memory alloys, we refer the reader to [4, Chapter 5]. Denoting by u the displacement and by θ the local temperature, we have

$$\rho_1 u_{tt} + \epsilon_1 u_t + \gamma u_{xxxx} - (\alpha\theta u_{1x} + \psi(u_x))_x = \rho_1 g \text{ in } (0, L_1) \times (0, T] \tag{1}$$

*Department of Mathematics, Faculty of Education, Gifu University, Gifu 501-1193, Japan

†Department of Mathematics and Computer Science, Eindhoven University of Technology, P.O. Box 513, 5600 MB Eindhoven, The Netherlands

‡Department of Mathematics and Computer Science, Eindhoven University of Technology, P.O. Box 513, 5600 MB Eindhoven, The Netherlands

[1]For a list of concrete applications of SMA see, for instance, the official homepage of the DFG initiative SFB 459 `http://www.ruhr-uni-bochum.de/sfb459` and the homepage of the TU Berlin "Shape Memory Alloys" group `http://www.smaterial.com/SMA`.

$$m\ell''(t) + \epsilon_2 m\ell'(t) = mg + \kappa\frac{L-(L_1+L_2)}{L_2} + \gamma u_{xxx}(t,L_1-) - (\alpha\theta u_x + \psi(u_x))(t,L_1-) + \kappa\frac{L_1-\ell(t)}{L_2}, \quad (2)$$

together with the boundary conditions

$$u(t,0) = 0, \quad (3)$$
$$u_{xx}(t,0) = u_{xx}(t,L_1) = 0, \quad (4)$$
$$u(t,L_1) = \ell(t) - L_1, \quad (5)$$

as well as the initial conditions

$$u_0(0,x) = \frac{\ell(0)-L_1}{L_1}x, \quad (6)$$
$$u_t(0,x) = 0, \quad (7)$$
$$\ell(0) = \ell_0, \quad (8)$$
$$\ell'(0) = 0. \quad (9)$$

All parameters entering (1)–(9) are strictly positive. ϵ_1, ϵ_2 and γ are small regularizing parameters, m is the mass of the joint of two springs, g is the gravitational acceleration, κ is the thermal conductivity of the SMA spring, u_0 is the initial displacement. The parameter α and the function $\psi(\cdot)$ incorporate the shape-memory effect. Cf. [4, pp. 179–181], $\psi(\cdot)$ is a sort of shear stress which is assumed to be proportional to the Devonshire Ansatz of the free energy density. The typical example of ψ is as follows (see Figure 2):

$$\psi(r) = \alpha_1 r - \alpha_2 r^3 + \alpha_3 r^5,$$

where α_1, α_2 and α_3 are positive constants. Both functions ψ and ψ' have been scaled in the figure with the parameter α. L_1 and L_2 denote the original length of the SMA and the linear elastic springs, respectively, and L is the length of a device (see Figure 1) that is used as a part of a valve of a rice cooking machine[2].

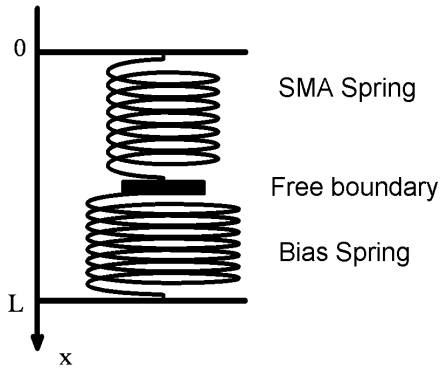

Figure 1: Sketch of the two-springs device.

Remark 1

a) (4) can be interpreted as "zero acceleration" or "no force" boundary condition.

[2]Note that in the case of such a device the role of the SMA spring is either to open the valve when the temperature in the cooking bath (and therefore also, via heat conduction, in the SMA spring) has entered a critical range or to keep the valve closed until the local temperature (in the SMA spring) is away from the critical range allowing for the SMA effect.

b) The physical situation described above corresponds to the geometric restriction

$$L_1 + L_2 > L. \tag{10}$$

Our general aim is to investigate intrinsic instabilities occurring when solving (1)–(9) numerically. Motivated by this we start our investigation by exploring here a 'skeleton' of our SMA model describing the motion of a shape-memory alloy spring at a small particular characteristic time scale. We call this scenario *fast-temperature-activation limit*. When speaking about fast-temperature-activation limit, we mean situations when the characteristic timescale $t_m = \sqrt{\frac{\rho_1 x_m^2}{\alpha\theta_m}}$ is fast[3]; see Appendix A for details. This corresponds to the limit case $\alpha \to \infty$. At this level, the standard Falk's model [2, 1, 4] reduces to a nonlinear elliptic partial differential equation (PDE) with a nonstandard Newton-type boundary condition.

The limit case $\alpha \to \infty$ is rather restricted and does not capture e.g. oscillations. We also study the simplest extension of the reduced model (11)–(15), namely the limit case $\rho_1 \to 0$, which involves oscillations and present numerical results for the resulting coupled ODE-PDE system.

This note is organized as follows: In Section 2, we show existence and uniqueness of a bounded weak solution and approximate this numerically in 1D. A well-posed numerical scheme is proposed in Section 3. This section also contains a couple of numerical illustrations. Section 4 contains the limiting PDE system (that captures now effects in the presence of two characteristic time scales) obtained by taking formally $\rho_1 \to 0$ in (1)–(9) as well as a corresponding numerical scheme and simulation results. We list in Appendix A the relevant characteristic timescales corresponding to (1)–(9).

2 SMA model in its fast-temperature-activation limit

If we pass to the limit $\alpha \to \infty$ in (1)–(9), we (formally) obtain as limit situation the following nonlinear PDE: For $t > 0$,

$$-(\theta u_x + \frac{1}{\alpha}\psi(u_x))_x = 0 \text{ in } (0, L_1), \tag{11}$$

$$\frac{\kappa}{\alpha}\frac{L - (L_1 + L_2)}{L_2} - \left(\theta u_x + \frac{1}{\alpha}\psi(u_x)\right)(t, L_1) + \frac{\kappa}{\alpha}\frac{L_1 - \ell(t)}{L_2} = 0, \tag{12}$$

together with the boundary conditions

$$u(t, 0) = 0 \tag{13}$$

$$u(t, L_1) = \ell(t) - L_1, \tag{14}$$

and with the initial condition

$$\ell(0) = \ell_0. \tag{15}$$

We refer to (11)–(15) as the *reduced model*.

2.1 List of assumptions

(A1) $\psi(r) = \psi_1(r) + \psi_2(r)$, $\psi_1(r)$ is a monotone increasing and locally Lipschitz continuous function satisfying $\psi_1(0) = 0$ and

$$\psi_1(r) \geq c|r|^q \text{ for any } r \in \mathbb{R}, |\psi_1(r) - \psi_1(r')| \leq L(M)|r - r'| \text{ for } M > 0, |r|, |r'| \leq M,$$

where $q \geq 2$ and c is a positive constant, $L(M)$ is a positive constant depending on M, and $\psi_2 \in C^2(\mathbb{R})$ and ψ_2 and ψ_2' are Lipschitz continuous on $\mathbb{R}$ satisfying

$$|\psi_2(r)| \leq C_\psi(|r| + 1), |\psi_2'(r) - \psi_2'(r')| \leq C_\psi|r - r'| \text{ for } r, r' \in \mathbb{R},$$

where C_ψ is a positive constant.

[3] Here "fast" actually means "close-to-zero".

(A2) $\theta \in W^{1,\infty}(0, L_1) \cap L^{\infty}_{+}(0, L_1)$ and $\theta \geq \theta_c$ on $(0, L_1)$ for some strictly positive constant θ_c.

(A3) $\alpha, \kappa, L_1, L_2, L \in \mathbb{R}^{*}_{+}$.

It is worth noting that assumptions (A1) – (A3) are consistent with the physical scenario in question. Particularly, observe that assumption (A1) permits the use of the standard forms of ψ mentioned in [4], e.g.

We refer to the system (11)–(15) as problem (P). For our convenience, we denote $H = L^2(0, L_1)$, $(u, v) = \int_0^{L_1} uv\, dx$ and

$$V := \{v \in H^1(0, L_1) : v(0) = 0\}$$

as the space for test functions. The weak formulation of the problem (P) is described below:

Definition 1 *Find $u \in V \cap H^2(0, L_1)$ such that*

$$(\theta u_x + \frac{1}{\alpha}\psi(u_x), \eta_x) + \frac{\kappa}{\alpha L_2} u(L_1)\eta(L_1) = \frac{\kappa}{\alpha L_2}(L - L_1 - L_2)\eta(L_1) \tag{16}$$

holds for all $\eta \in V$.

Theorem 1 *Assume (A1)–(A3) be fulfilled. If α is sufficiently large, then there exists at least a weak solution $u \in V \cap H^2(0, L_1)$ to the problem (P).*

2.2 Existence and uniqueness of weak solutions to (11)–(15)

First, we consider the following problem P0(θ, f, g) for a given function f and a constant g:

$$\begin{aligned}
&-(\theta u_x + \frac{1}{\alpha}\psi_1(u_x))_x = f \text{ in } (0, L_1),\\
&-\frac{\kappa}{\alpha L_2} u(L_1) - (\theta u_x + \frac{1}{\alpha}\psi_1(u_x))(L_1) = g,\\
&u(0) = 0,
\end{aligned}$$

where $f \in H$ and $g \in \mathbb{R}$.

In order to show the existence of a solution of P0(θ, f, g) we set

$$\mathcal{A} : D(A) = V \cap \{z \in H^2(0, L_1) : -\frac{\kappa}{\alpha L_2} z(L_1) - (\theta z_x + \frac{1}{\alpha}\psi_1(z_x))(L_1) = g\} \to H$$

by

$$\mathcal{A}z = -(\theta z_x + \frac{1}{\alpha}\psi_1(z_x))_x \text{ for } z \in D(\mathcal{A}).$$

It is clear that $\mathcal{A}$ is monotone and demicontinuous so that $\mathcal{A}$ is a maximal monotone operator. Moreover, by (A1) and (A2) $\mathcal{A}$ is coercive on H. Then we can obtain the following lemma:

Lemma 1 *[3, Chapter 1, Theorem 1.4] Assume (A1) - (A3), $f \in H$ and $g \in \mathbb{R}$. Then there exists one and only one $u \in D(A)$ such that u is a weak solution of P0(θ, f, g).*

Now, we provide a proof of Theorem 1.

Proof. For $M > 0$ we put

$$K(M) = \{z \in H^2(0, L_1) : |z|_{H^2(0,L_1)} \leq M\}.$$

Let $w \in K(M)$, $f = \frac{1}{\alpha}\psi_2(w_x)_x$ and $g = \frac{\kappa}{\alpha L_2}(L - L_1 - L_2) + \frac{1}{\alpha}\psi_2(w_x)(L_1)$. Then Lemma 1 implies that P0(θ, f, g) has a unique solution $u \in D(\mathcal{A})$. Now, we denote by $S : K(M) \to D(A)$ this solution operator.

As the first step of this proof we shall show the existence of a large number M such that $S : K(M) \to K(M)$. In fact, let $M > 0$, $w \in K(M)$ and $u = Sw$. Then, by taking u as a test function we have

$$\begin{aligned} & (\theta u_x + \frac{1}{\alpha}\psi_1(u_x), u_x) + \frac{\kappa}{\alpha L_1}|u(L_1)|^2 \\ = \quad & (\frac{1}{\alpha}\psi_2(w_x), u_x) + (\frac{\kappa}{\alpha}L_0 + \frac{1}{\alpha}\psi_2(w_x)(L_1))u(L_1), \end{aligned}$$

where $L_0 = \frac{L-(L_1+L_2)}{L_2}$.

Here, we give the following useful inequality:

$$|z|_H \le C_*|z_x|_H \text{ for } z \in V, |z_x(L_1)| \le C_*|z|_{H^2(0,L_1)} \text{ for } z \in H^2(0, L_1), \tag{17}$$

where C_* is a positive constant. Immediately, we see that

$$\begin{aligned} & \theta_c|u_x|_H^2 + \frac{c}{\alpha}\int_0^{L_1} |u_x|^q dx + \frac{\kappa}{\alpha L_2}|u(L_1)|^2 \\ \le \quad & \frac{C_\psi}{\alpha}(|w_x|_H + \sqrt{L_1})|u_x|_H + (|\frac{\kappa}{\alpha}L_0| + \frac{C_\psi}{\alpha}(|w_x(L_1)| + 1)|u(L_1)| \\ \le \quad & \frac{\theta_c}{2}|u_x|_H^2 + \frac{C_\psi^2}{\alpha^2\theta_c}(|w_x|_H^2 + L_1) + \frac{\kappa}{2\alpha L_2}|u(L_1)|^2 + \frac{C_\psi^2 L_2}{\alpha\kappa}(|w_x(L_1)|^2 + 1). \end{aligned}$$

By choosing $\alpha \ge \frac{C_\psi^2}{\kappa}$, it holds that

$$\frac{\theta_c}{2}|u_x|_H^2 + \frac{c}{\alpha}\int_0^{L_1} |u_x|^q dx + \frac{\kappa}{2\alpha L_2}|u(L_1)|^2 \le \frac{C_\psi^2}{\alpha^2\theta_c}(|w_x|_H^2 + L_1) + L_2(|w_x(L_1)|^2 + 1) \tag{18}$$

so that on account of (17) $|u_x|_H \le \frac{1}{\sqrt{\alpha}}C(M+1)$ where C is a positive constant. Moreover, since $-(\theta u_x + \frac{1}{\alpha}\psi_1(u_x))_x = \frac{1}{\alpha}\psi_2(w_x)_x$ on $(0, L_1)$, we have

$$(\theta_c + \frac{1}{\alpha}\psi_1'(u_x))|u_{xx}| \le |\theta_x u_x| + \frac{1}{\alpha}|\psi_2(w_x)_x| \text{ on } (0, L_1).$$

By using (A1) we observe that

$$|u_{xx}|_H \le \frac{1}{\theta_c}(|\theta_x|_{L^\infty(0,L_1)}|u_x|_H + \frac{C_\psi}{\alpha}|w_{xx}|_H) \le \frac{1}{\theta_c}(\frac{C}{\sqrt{\alpha}}(M+1)|\theta_x|_{L^\infty(0,L_1)} + \frac{C_\psi}{\alpha}M).$$

Therefore, there exist positive constants M and α such that $S : K(M) \to K(M)$. Immediately, this guarantees the following estimate:

$$|u_x|_{L^\infty(0,L_1)} \le C_1 \text{ for } u = Sw, w \in K(M),$$

where C_1 is some positive constant.

In the next step, let $w_1, w_2 \in K(M)$, $u_i = Sw_i$, $i = 1, 2$, $w = w_1 - w_2$, and $u = u_1 - u_2$. Then, it holds that

$$\begin{aligned} & -(\theta u_x)_x - (\frac{1}{\alpha}\psi_1(u_{1x}) - \frac{1}{\alpha}\psi_1(u_{2x}))_x = (\frac{1}{\alpha}\psi_2(u_{1x}) - \frac{1}{\alpha}\psi_2(u_{2x}))_x \text{ in } (0, L_1), \\ & -\frac{\kappa}{\alpha L_2}u(L_1) - (\theta u_x + \frac{1}{\alpha}(\psi_1(u_{1x}) - \psi_1(u_{2x}))(L_1) = \frac{1}{\alpha}(\psi_2(u_{1x}) - \psi_2(u_{2x}))(L_1), \\ & u(0) = 0. \end{aligned}$$

Similarly to (18), we can obtain

$$\begin{aligned} \theta_c|u_x|_H^2 + \frac{\kappa}{\alpha L_2}|u(L_1)|^2 \quad & \le \quad \frac{C_\psi}{\alpha}|w_x|_H|u_x|_H \\ & \le \quad \frac{\theta_c}{2}|u_x|_H^2 + \frac{C_\psi^2}{2\alpha^2}|w_x|_H^2 \end{aligned}$$

so that

$$\frac{\theta_c}{2}|u_x|_H^2 \leq \frac{C_\psi^2}{2\alpha^2}|w_x|_H^2. \tag{19}$$

Furthermore, since

$$\begin{aligned} & -(\theta + \frac{1}{\alpha}\psi_1'(u_{1x}))u_{xx} \\ = \quad & \theta_x u_x + \frac{1}{\alpha}(\psi_1'(u_{1x}) - \psi_1'(u_{2x}))u_{2xx} + \frac{1}{\alpha}\psi_2'(w_{1x})w_{xx} + \frac{1}{\alpha}(\psi_2'(w_{1x}) - \psi_2'(w_{2x}))w_{2xx} \text{ on } (0, L_1), \end{aligned}$$

we observe

$$\theta_c|u_{xx}|_H \leq |\theta_x|_{L^\infty(0,L_1)}|u_x|_H + \frac{L(C_1)}{\alpha}|u_x|_{L^\infty(0,L_1)}|u_{2xx}|_H + \frac{C_\psi}{\alpha}(|w_{xx}|_H + |w_x|_{L^\infty(0,L_1)}|w_{2xx}|_H).$$

Therefore, for sufficiently large α S is a contraction mapping. Thus we have proved Theorem 1. ■

Theorem 2 *Under the assumptions (A1)–(A3) and $\alpha > \frac{C_\psi^2}{\theta_c}$, problem (P) has a unique weak solution.*

Proof. Let u_1 and u_2 be solutions of (P) and $u = u_1 - u_2$. Then in the similar way to that of (19) we have

$$\frac{\theta_c}{2}|u_x|_H^2 \leq \frac{C_\psi^2}{2\alpha^2}|u_x|_H^2.$$

This implies the uniqueness of a solution to (P). ■

3 Numerical scheme and simulation results

In this section we solve the boundary value problem (11)–(15) numerically. We consider the reduced model, posed in $(0, L_1)$, in the form

$$\theta_x(t,\cdot)u_x + \left(\theta(t,\cdot) + \frac{1}{\alpha}\psi'(u_x)\right)u_{xx} = 0, \tag{20}$$

with the boundary conditions

$$u(0) = 0, \tag{21}$$

$$u(L_1) = \ell(t) - L_1, \tag{22}$$

where ℓ is defined as

$$\ell(t) := L_1 - \frac{\alpha L_2}{\kappa}\left(\theta(t,\cdot)u_x + \frac{1}{\alpha}\psi'(u_x)\right)\Big|_{x=L_1} + L - L_1 - L_2. \tag{23}$$

We choose a uniform grid with $N+1$ grid points, say $x_i = (i-1)h$, $i = 1, 2, \ldots, N+1$, where $h = L_1/N$. We denote the numerical approximation for $u(x_i)$ by u_i and we shall write $\theta(t, x_i) = \theta_i(t)$. Using central difference approximations for all derivatives in (20) we find the following equation at all internal grid points, i.e., for $i = 2, 3, \ldots, N$:

$$\theta_{x,i}(t)\frac{u_{i+1} - u_{i-1}}{2h} + \left(\theta_i(t) + \frac{1}{\alpha}\psi'\left(\frac{u_{i+1} - u_{i-1}}{2h}\right)\right)\frac{u_{i+1} - 2u_i + u_{i-1}}{h^2} = 0. \tag{24}$$

The boundary conditions (21) give for $i = 1$

$$u_1 = 0, \tag{25}$$

and, if we discretize $u_x(x_{N+1})$ with a backward difference, for $i = N + 1$

$$u_{N+1} = -\frac{\alpha L_2}{\kappa}\left(\theta_i \frac{u_{N+1} - u_N}{h} + \frac{1}{\alpha}\psi'\left(\frac{u_{N+1} - u_N}{h}\right)\right) + L - L_1 - L_2. \tag{26}$$

Equations (24)–(26) form a system of $N + 1$ nonlinear equations for the $N + 1$ unknowns u_1, u_2, $\ldots$, u_{N+1}. Defining the vector $\boldsymbol{u} := (u_1, u_2, \ldots, u_{N+1})^T$, we may write this system as $\boldsymbol{f}(\boldsymbol{u}) = \boldsymbol{0}$. This nonlinear system can be solved using standard Newton iteration. It is worth noting that the locally Lipschitz property of ψ' ensures the local existence of the discrete solution.

For our numerical results, we have used the following parameter values. We set $\alpha = 1/50 \cdot 10^9$, $\kappa = 0.8 \cdot 10^9$, $L_1 = L_2 = 0.01$ and $L = 0.015$. Furthermore we take

$$\frac{\psi(r)}{\alpha} = \left(-\frac{1}{5}r - 2r^3 + r^5\right) \cdot 50, \tag{27}$$

for all $r \in [r_{\min}, r_{\max}]$ and assume that the temperature profile θ is given by $\theta(t, x) = 80t + 20$.

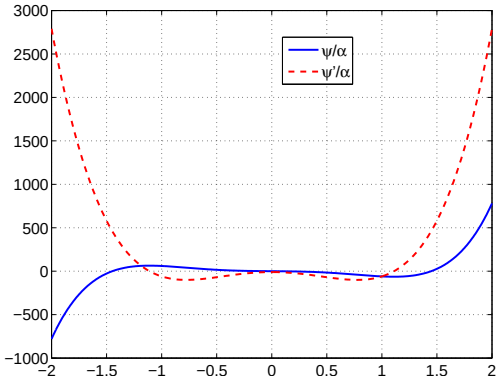

Figure 2: Graphs of ψ/α and ψ'/α for $r_{\min} = -2$ and $r_{\max} = 2$.

See Figure 2 for the typical graphs of ψ/α and ψ'/α. Note that we have scaled both functions with α. Finally, we use $N = 40$ grid points and we perform Newton iteration steps to solve the nonlinear system until the residual is smaller than 10^{-7}.

Note that the time t is only a parameter in the equations in this section. We have solved the nonlinear system for values of t equal to $t_k = k/1000$, $k = 0, 1, \ldots, 1000$. The numerical results are presented in Figure 3. In the left figure we see u as a function of the spatial coordinate x for the different values of t. Note that the dependence of u on x is apparently linear, since each graph is a straight line. In the right figure we see ℓ as a function of time. Here, $\ell = \ell(t)$ is computed as $\ell = u_{N+1} + L_1$ for each value of t. The graph shows that the valve opens in an instant so that this behavior of the free boundary is realistic. The opening of the valve occurs at $t = 0.26$.

Please note that the behavior is lost if we take different coefficients in (27) that lead to a monotonic function ψ. If ψ is monotonic, the valve will not open rapidly. If we redo the simulation for parameter values $\alpha = 1/8 \cdot 10^9$, $\kappa = 10^9$, and

$$\frac{\psi(r)}{\alpha} = \left(\frac{130}{8}r - 2r^3 + r^5\right) \cdot 8, \tag{28}$$

we obtain the graphs in Figure 4. Indeed, we observe in Figure 4 that ℓ is almost linear. The shape of ψ as in Figure 2 is essential for the shape memory effect to occur.

The shooting method (cf. [5], e.g.) gives a simple alternative approach to solve the current problem. Indeed, since θ does not depend on the spatial coordinate, we find from

$$f(u_x) = \theta u_x + \frac{1}{\alpha}\psi(u_x)(=: f(s)), \tag{29}$$

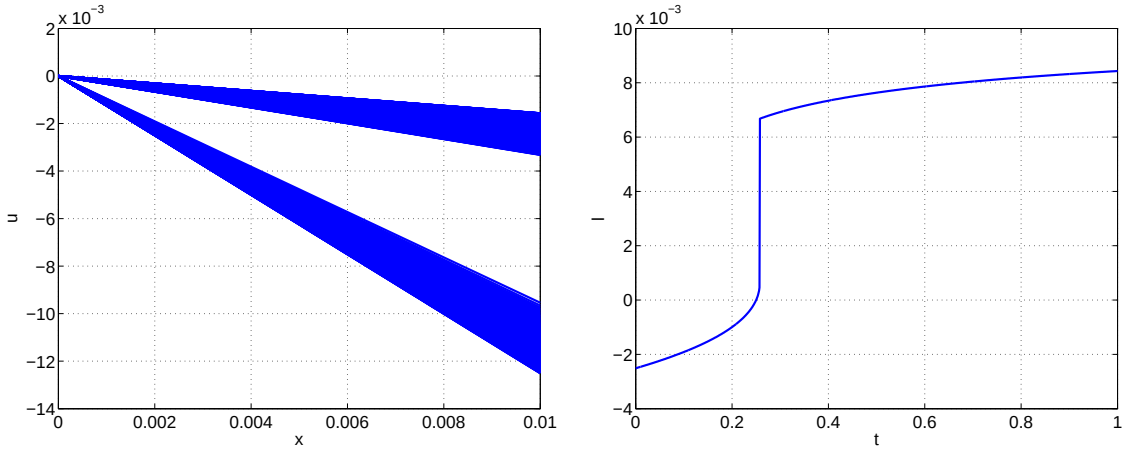

Figure 3: Displacement u as a function of the spatial coordinate x for given values of t (left). Position of the valve ℓ as a function of time t (right).

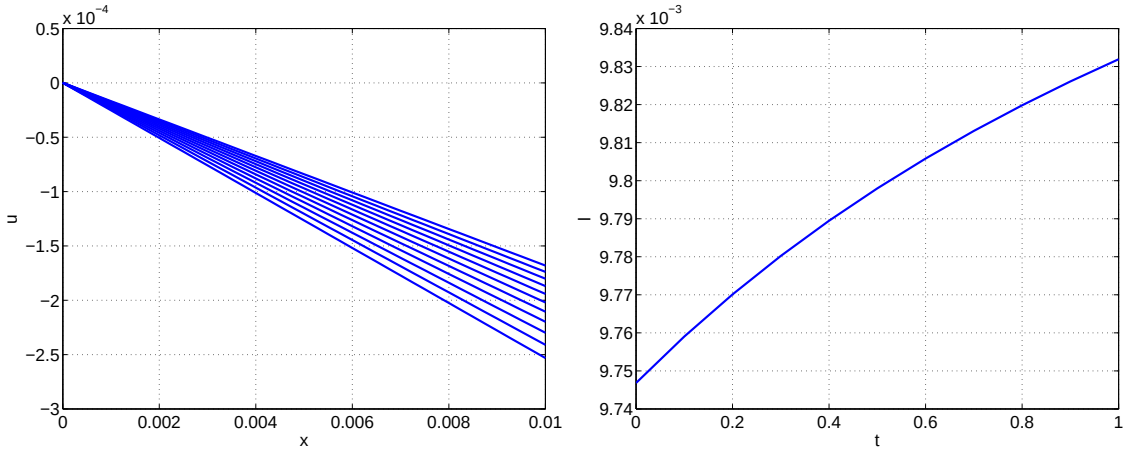

Figure 4: Displacement u as a function of the spatial coordinate x for given values of t (left). Position of the valve ℓ as a function of time t (right). Monotonic ψ.

that u_x is constant throughout the interval[4]. Hence $u_x(x) = u_x(0) = s$ for all $x \in (0, L_1)$. Integrating, we find $u(x) = sx$. Now if we want the solution to satisfy the original boundary condition at $x = L_1$, we need to choose s such that

$$\theta s + \frac{1}{\alpha}\psi(s) = \frac{\kappa}{\alpha L_2}\left(L - L_1 - L_2 - sL_1\right). \tag{30}$$

Setting

$$F(s) := \theta s + \frac{1}{\alpha}\psi(s) - \frac{\kappa}{\alpha L_2}\left(L - L_1 - L_2 - sL_1\right), \tag{31}$$

we see that we can also find a numerical approximation of the displacement u by finding the zero of F. Note that the shooting approach is computationally much cheaper than discretizing the PDE and solving the full nonlinear system $\boldsymbol{f}(\boldsymbol{u}) = \boldsymbol{0}$. Indeed we only need to solve the scalar equation $F(s) = 0$ at each time t. The numerical results obtained are of course identical in both the discretization and the shooting method.

4 An extension of the reduced model (11)–(15)

The limit case that we have considered so far, $\alpha \to \infty$, is rather restricted and does not capture yet oscillations. We study here the simplest extension of the reduced model (11)–(15), namely the limit case $\rho_1 \to 0$, which involves oscillations. In this situation, the initial PDE system reduces to

$$(\gamma u_{xxx} - \alpha f(u_x))_x = 0 \text{ in } (0, L_1), \tag{32}$$

$$m\ell''(t) = mg + \frac{\kappa}{L_2}(L - L_2 - \ell(t)) + (\gamma u_{xxx} - \alpha f(u_x))|_{x=L_1}, \tag{33}$$

to which we add the following boundary conditions for u and initial conditions for ℓ:

$$\begin{aligned}
u(t,0) &= 0, && (34)\\
u_{xx}(t,0) &= u_{xx}(t,L_1) = 0, && (35)\\
u(t,L_1) &= \ell(t) - L_1, && (36)\\
\ell(0) &= \ell_0, && (37)\\
\ell'(0) &= 0. && (38)
\end{aligned}$$

The presence of the terms γu_{xxxx} and $m\ell''$ introduce novel behaviors compared to those captured in the approximation $\alpha \to \infty$. To study (32)–(38), it is convenient to introduce an additional unknown for this problem, namely $w := u_{xx}$. Hence the system (32)–(38) is equivalent to (39)–(46), viz.

$$\begin{aligned}
-u_{xx} &= -w && (39)\\
-\gamma w_{xx} &= -\alpha f'(u_x) w && (40)\\
m\ell''(t) &= mg + \frac{\kappa}{L_2}(L - L_2 - \ell(t)) + (\gamma w_x - f(u_x))|_{x=L_1}, && (41)
\end{aligned}$$

with

$$\begin{aligned}
u(t,0) &= 0, && (42)\\
w(t,0) &= w(t,L_1) = 0, && (43)\\
u(t,L_1) &= \ell(t) - L_1, && (44)\\
\ell(0) &= \ell_0, && (45)\\
\ell'(0) &= 0. && (46)
\end{aligned}$$

[4]Note that if $f(s)$ were monotonic in s, then the shooting method can also provide a way to prove uniqueness of the discrete approximation.

We postpone the study of the well-posedness of (39)–(46) to a later moment and investigate only how its discrete approximation responds to the oscillations introduced by the differential equation for $\ell(t)$, namely by (41). However, we expect that the main ideas used in Section 2.2 to get the existence and uniqueness of a weak solution to problem (P) also apply for the ODE-PDE system.

We propose the following numerical scheme: we rewrite (41) as a system of first order ODEs in the standard way. Hence we introduce $(\ell_1, \ell_2) := (\ell, \ell')$. By definition and (41) we now have

$$\ell_1' = \ell_2, \tag{47}$$

$$\ell_2' = g + \frac{\kappa}{mL_2}(L - L_2 - \ell_1(t)) + \frac{1}{m}(\gamma w_x - f(u_x))|_{x=L_1}. \tag{48}$$

This system can be solved using standard ODE solvers. To evaluate the right hand side of (48) we discretize PDEs (39) and (40) and solve the resulting nonlinear system using Newton iteration. This is similar to the method detailed in Section 3.

The inclusion of the ODE for ℓ leads to high frequency oscillations. Since we are interested in long time behavior of the solution, we add a damping term to (48), viz.

$$\ell_2' = -\epsilon\ell_2 + g + \frac{\kappa}{mL_2}(L - L_2 - \ell_1(t)) + \frac{1}{m}(\gamma w_x - f(u_x))|_{x=L_1}. \tag{49}$$

By numerical simulations we find $\epsilon = 10^7$ to be an appropriate value to "kill" the oscillations. In Figure 5 we illustrate this by showing l as a function of time for the initial condition $l_0 = -10^3$ and on the time interval $(0, 10^{-6})$. All other parameter values are chosen as in Section 3 (the non-monotonic choice for ψ, cf. (27)). The results are for $\epsilon = 0$ (no damping) and $\epsilon = 10^7$ (damping). As ODE solver we have used Matlab's built-in `ode15s` routine. This is a variable order multistep solver based on the numerical differentiation formulas (NDFs) which is especially suited for stiff equations as those we encounter here.

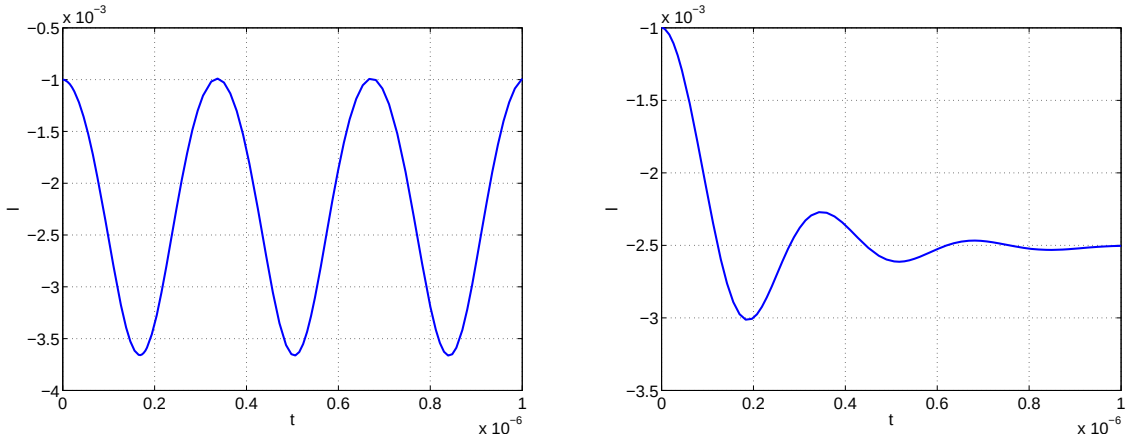

Figure 5: Position of the valve ℓ as a function of time t; no damping (left) and damping (right). Short-time behavior.

The initial oscillations will also be smaller if we start close to the equilibrium position. The results for a simulation on the full time domain $(0, 1)$ starting with the initial condition $l_0 = -2.5 \cdot 10^{-3}$ (which is near the equilibrium position of the valve) is presented in Figure 6. Please note the similarity with Figure 3 (right). We do not show graphs of the displacement u here – as before, we find that u is a linear function of x and, correspondingly, we see in our simulations that $w = u_{xx} = 0$.

Remark 2 *The oscillations in Figure 5 (left) are not only caused by the term $-(\kappa/(mL_2))\ell_1(t)$ in the right hand side of* (49)*. Indeed, this term would lead to oscillations with a frequency $f_{hom} = \sqrt{\kappa/(mL_2)}/(2\pi) \approx$*

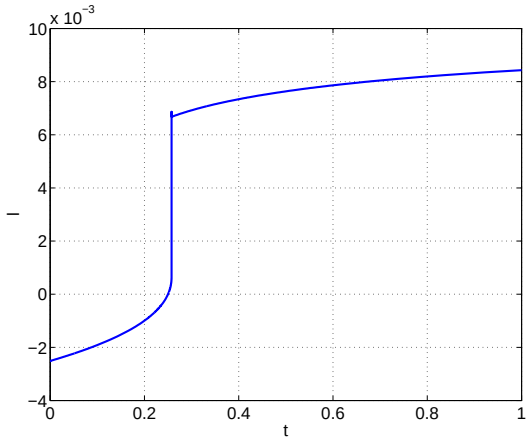

Figure 6: Position of the valve ℓ as a function of time t. Long-time behavior.

$1.4 \cdot 10^6$, *that is clearly lower than the frequency of the oscillations in Figure 5 (left). If we remove the last term in the right hand side of* (49), *i.e., replace* (49) *by*

$$\ell_2' = -\epsilon \ell_2 + g + \frac{\kappa}{mL_2}(L - L_2 - \ell_1(t)), \tag{50}$$

we do obtain oscillations with frequency f_{hom}.

A Characteristic timescales for (1)–(9)

Denoting by $[A]$ the unit of the quantity A, and by M, T, L, and K corresponding units for mass, time, space, and degrees Kelvin, we have: $[\rho_1] = ML^{-1}$, $[u_1] = L$, $[\kappa] = MLT^{-2}$, $[\theta] = K$, $[g] = MT^{-2}$, $[\ell(t)] = L$, $[\epsilon_1] = ML^{-1}T^{-1}$, $[\epsilon_2] = T^{-1}$, $[\gamma] = ML^3T^{-2}$, $[\alpha] = MLT^{-2}K^{-1}$, $[\alpha_k] = ML^2T^{-2}$ (for all $k \in \{1, 2, 3\}$), and $[m] = M$.

Let u_m, t_m, x_m, and θ_m be reference displacement, characteristic time scale, characteristic length scale, and reference temperature, respectively. Denoting now $u_1 := u_m v$, $t := t_m t$, $x := x_m y$, $\ell(t) = x_m s(t)$, and $\theta := \theta_m T$, the differential system (1)–(9) becomes

$$\begin{aligned} v_{tt} &+ \frac{\epsilon_1 t_m}{\rho_1} v_t + \frac{\gamma t_m^2}{\rho_1 x_m^2} v_{yyyy} - \frac{\alpha \theta_m t_m^2}{\rho_1 x_m^2} (T v_y)_y \\ &- \frac{u_m \alpha_1 t_m^2}{x_m^3 \rho_1} \left(1 - 3\frac{\alpha_2}{\alpha_1}\frac{u_m^2}{x_m^2} v_y^2 + 5\frac{\alpha_3}{\alpha_1}\frac{u_m^4}{x_m^4} v_y^4\right) v_{yy} = \frac{t_m^2}{u_m} g, \end{aligned} \tag{51}$$

$$\begin{aligned} s''(t) &+ t_m \epsilon_2 s'(t) = \frac{t_m^2}{x_m} g + \frac{\kappa t_m^2}{m x_m} \frac{L - (L_1 + L_2)}{L_2} + \frac{t_m^2 u_m \gamma}{m x_m^4} v_{yyy} - \frac{t_m^2 \alpha \theta_m u_m}{m x_m^2} T v_y \\ &- \left(\frac{t_m^2 \alpha_1 u_m}{m x_m} v - \frac{t_m^2 \alpha_2 u_m^3}{m x_m} v^3 + \frac{t_m^2 \alpha_3 u_m^5}{m x_m} v^5\right) + \frac{t_m^2 \kappa}{m L_2}\left(\frac{L_1}{x_m} - s(t)\right) \end{aligned} \tag{52}$$

$$
\begin{aligned}
v_1(t,0) &= 0, && (53)\\
v_{yy}(t,0) &= v_{yy}(t,L_1) = 0, && (54)\\
v(t,\frac{L_1}{x_m}) &= \frac{x_m}{u_m}s(t) - \frac{L_1}{u_m}, && (55)\\
v_{10}(0,y) &= \frac{x_m s(0) - L_1}{L_1}y, && (56)\\
v_t(0,y) &= 0, && (57)\\
s(0) &= s_0 := \frac{\ell_0}{x_m}, && (58)\\
s'(0) &= 0. && (59)
\end{aligned}
$$

We have much freedom in choosing the reference temperature θ_m. It seems that a good choice of reference length scale is $x_m := L_1$, while a reference displacement may be given by $u_m := x_m$. It is not quite clear which characteristic time scale should one take for the numerical simulations. A first choice would be to take the "elastic" characteristic time scale $t_m := \sqrt{\frac{u_m}{g}}$.

(51) and (52) suggest a couple of other characteristic time scales, which are associated to further involved subprocesses. We list but five of them: the ϵ_1-damping characteristic time scale $t_m := \frac{\rho_1}{\epsilon_1}$, the ϵ_2-damping characteristic time scale $t_m := \frac{1}{\epsilon_2}$, the γ-regularization characteristic time scale $t_m := \sqrt{\frac{\rho_1 x_m^2}{\gamma}}$, the "temperature-activation" characteristic time scale $t_m := \sqrt{\frac{\rho_1 x_m^2}{\alpha\theta_m}}$, and the memory characteristic time scale $t_m := \sqrt{\frac{\rho_1 x_m^3}{u_m \alpha_1}}$.

References

[1] Aiki, T., A mathematical model for a valve made of a spring of a shape memory alloy. *Mathematical Aspects of Modeling Structure Formation Phenomena*, Gakuto, International Series Mathematical Sciences and Applications, **29** (2008), pp. 1–18.

[2] Aiki, T., Kenmochi, N., Some models for shape memory alloys, Gakuto, International Series Mathematical Sciences and Applications, *Mathematical Aspects of Modeling Structure Formation Phenomena*, pp. 144–162.

[3] Barbu, V., *Optimal Control of Variational Inequalities*. Pitman, Boston, 1984.

[4] Brokate, M., Sprekels, J., *Hysteresis and Phase Transitions*. Springer Verlag, Berlin, 1996.

[5] Stoer, J., Bulirsch. R, *Introduction to Numerical Analysis*. Springer-Verlag, NY, 1980.